


Influence of sulfide on diazotrophic growth of the methanogen *Methanococcus maripaludis* and its implications for the origin of nitrogenase

Devon Payne¹, Rachel L. Spietz ¹, Dennis L. Newell ², Paul Dijkstra³ & Eric S. Boyd ¹✉

Methanogens inhabit euxinic (sulfide-rich) or ferruginous (iron-rich) environments that promote the precipitation of transition metals as metal sulfides, such as pyrite, reducing metal or sulfur availability. Such environments have been common throughout Earth's history raising the question as to how anaerobes obtain(ed) these elements for the synthesis of enzyme cofactors. Here, we show a methanogen can synthesize molybdenum nitrogenase metallocofactors from pyrite as the source of iron and sulfur, enabling nitrogen fixation. Pyrite-grown, nitrogen-fixing cells grow faster and require 25-fold less molybdenum than cells grown under euxinic conditions. Growth yields are 3 to 8 times higher in cultures grown under ferruginous relative to euxinic conditions. Physiological, transcriptomic, and geochemical data indicate these observations are due to sulfide-promoted metal limitation, in particular molybdenum. These findings suggest that molybdenum nitrogenase may have originated in a ferruginous environment that titrated sulfide to form pyrite, facilitating the availability of sufficient iron, sulfur, and molybdenum for cofactor biosynthesis.

¹Department of Microbiology and Cell Biology, Montana State University, Bozeman, MT 59717, USA. ²Department of Geosciences, Utah State University, Logan, UT 84322, USA. ³Center for Ecosystem Science and Society and Department of Biological Sciences, Northern Arizona University, Flagstaff, AZ 86011, USA. ✉email: eric.boyd@montana.edu

Nitrogen (N) is essential for the synthesis of nucleic and amino acids and other key biomolecules in all forms of life. Earth's largest reservoir of N is dinitrogen (N_2) gas in the atmosphere; however, it is not bioavailable and must be fixed to nitrate (NO_3^-) or ammonia (NH_3) prior to its assimilation. As such, the availability of fixed N often limits the productivity of ecosystems¹. On early Earth, fixed N is thought to have been supplied by abiotic processes such as lightning-based oxidation of atmospheric N_2 or mineral reduction of N_2 ^{2,3}. However, fixed N from these sources would have been minimal and finite, and together these features are thought to have limited ecosystem productivity during this time¹. Today, approximately 50% of all fixed N is generated through the biological process of N_2 fixation^{1,4}, whereby N_2 is reduced to NH_3 by the enzyme nitrogenase (diazotrophy) with the remaining fixed N largely generated through the industrial Haber-Bosch process.

Three different forms of nitrogenase have been described to date and these are differentiated by the (hetero)metals comprising the active site of each enzyme complex⁵. This includes molybdenum (Mo), vanadium (V), and iron (Fe)-only forms of nitrogenase^{6,7}. Mo-nitrogenase (Nif) is taxonomically the most widely distributed and oldest form of nitrogenase^{8,9} and, at a minimum, consists of the structural proteins NifHDK and maturase proteins, NifB(E)N¹⁰. The active site metallocluster of Nif comprises a six iron (Fe) and nine sulfur (S) atom core with Fe symmetrically coordinating a central carbon atom; the metallocluster is capped by Fe and Mo atoms [7Fe-Mo-9S] (termed the FeMo-cofactor^{10,11}). In addition to FeMo-cofactor(s), Nif requires the complex P-cluster that consists of eight Fe atoms and seven S atoms [8Fe-7S]¹². A FeMo-cofactor is housed within each NifD structural protein, whereas the P-cluster is found at the interface of each NifD and NifK, ultimately forming the heterotetramer, NifD₂K₂¹³. Dinitrogenase reductase, NifH, modulates the ATP-dependent transfer of electrons to NifD₂K₂ and it harbors an additional [4Fe-4S] cluster for each of two NifH subunits^{14,15}. Thus, cells performing N_2 -fixation via Nif have a high demand for Fe, S, Mo, ATP, and reducing equivalents.

Phylogenetic analyses of a concatenation of NifHDK proteins indicate that the earliest evolving lineages of Nif are found in hydrogenotrophic methanogens^{6-9,16,17}. These observations are corroborated by other data indicating NifHDK evolved from a series of duplications of genes encoding an ancestor of CfbCD⁸, proteins that are required to synthesize cofactor F₄₃₀^{18,19}. That F₄₃₀ (and CfbCD encoding genes) are exclusively found in archaeal methanogens (and archaeal alkanotrophs)²⁰ is further evidence indicating an origin for Nif among ancestors of these Archaea. These data have been used to suggest an origin for Nif among an ancestor of anaerobic methanogens during the mid-Paleoproterozoic ~1.8–2.1 billion years ago (Ga)^{6,9,17}, although isotopic data of organic matter preserved in shales dated to >3 Ga suggest an even earlier origin^{21,22}. Regardless of the actual date of its origin, nitrogenase is interpreted to be an ancient enzyme that originated in an anoxic environment on early Earth. An anoxic origin for this enzyme is consistent with the oxygen-sensitivity of the metal clusters required for Nif function²³. Nif then diversified among anaerobes and only late in its evolutionary history was it acquired via horizontal gene transfer among organisms capable of integrating oxygen (O_2) into their energy metabolism or capable of producing O_2 in the case of Cyanobacteria. Expanded biological productivity associated with the proliferation of Cyanobacteria and O_2 production would have increased demand for existing abiotic pools of fixed N²⁴, which may have been the selective pressure to evolve a biological mechanism to reduce atmospheric N_2 and relieve N limitation^{7,25}.

Ferruginous conditions (anoxic and ferrous iron (Fe(II))-rich) likely dominated anoxic environments during the Archean

(>2.4 Ga)^{26,27}. This is due to the circulation of hydrothermal fluids through iron-rich mid-ocean basalts, which led to input of a greater amount of Fe(II) into anoxic ocean basin waters than sulfide (HS^-)²⁸. In the absence of oxygen, the excess Fe(II) would have been stable, and free Fe(II) concentrations are estimated to have ranged from 0.05 to 0.5 mM²⁹. However, the proliferation of Cyanobacteria and the production of O_2 during the late Archean drove the oxidative weathering of continental sulfide minerals that increased the flux of sulfate into oceans. When combined with increased productivity near ocean margins^{30,31}, this would have stimulated heterotrophic sulfate reduction and HS^- production. In turn, this led to stratified coastal oceans that were oxygenated at the surface and were euxinic (anoxic and HS^- -rich) at depth³⁰⁻³². In contrast, deeper ocean waters and those more distal from continental margins remained ferruginous²⁶, due to lower productivity in the overlying water column, decreased availability of sulfate and subsequent heterotrophic sulfate reduction, and hydrothermal input of Fe^{26,33,34}. HS^- has a high affinity for Fe(II), resulting in the formation of low-solubility iron-sulfide minerals, including pyrite (FeS_2)³⁵⁻³⁷. As such, in euxinic environments, concentrations of HS^- exceed that of Fe(II), resulting in the titration and precipitation of Fe(II) as FeS_2 . Under these conditions, excess HS^- is also available to complex with other thiophilic metals (e.g., Mo, Co, Ni), potentially rendering them less bioavailable^{33,34,38}.

How might N_2 -fixing methanogens have met their concurrent demands for Fe, S, and Mo for the synthesis of Nif cofactors during the Paleoproterozoic or even earlier, when one or more of these elements were likely to be of limited availability due to the tendency for metal sulfide formation? Potential clues come from recent studies of contemporary methanogens, specifically *Methanococcus voltae* and *Methanosarcina barkeri*, that reveal their ability to reductively dissolve FeS_2 and utilize dissolution products to meet Fe and S nutritional demands³⁹⁻⁴¹. *M. voltae* and *M. barkeri* grown with FeS_2 had similar growth rates and cell yields when compared to traditional sources of Fe and S used to grow methanogens (Fe(II) and HS^- and/or cysteine)^{39,40}. However, these experiments were conducted on non- N_2 -fixing methanogen cells, which would be expected to have a lower demand for Fe, S, and Mo than those actively fixing N_2 , in particular those growing with Mo-nitrogenase. Such observations point to ferruginous conditions as being possibly more favorable than euxinic conditions for the origin and early proliferation of Nif.

Here, we sought to evaluate the effect of euxinic and ferruginous conditions on the growth and activity of the methanogen, *Methanococcus maripaludis* S2 (MmS2), to provide new insights into the environment type most conducive for the origin of Nif. Cells were first grown with Fe(II) and HS^- or FeS_2 as a primary Fe and S source under N_2 -fixing or NH_3 -amended conditions, to establish whether FeS_2 could serve as a Fe and S source for biosynthesis of nitrogenase and to determine whether HS^- drives Mo limitation. Cultivation assays were then focused on FeS_2 -grown cells, since this condition allows for excess Fe(II) or HS^- to be included in the cultivation medium thereby permitting an evaluation of the effect of ferruginous or euxinic conditions, respectively, on metal availability and N_2 fixation activity. Nif is the only nitrogenase encoded in MmS2⁴², mitigating the confounding variable associated with cells switching to more recently evolved and alternative forms of nitrogenase (i.e., Fe-nitrogenase Anf; V-nitrogenase, Vnf⁹) if, or when, Mo becomes limiting^{5,43}. Further, the Nif encoded by MmS2 belongs to the earliest evolving lineage of nitrogenase^{6,8,9,16}. To place additional Mo demands on MmS2, cells were grown with formate, requiring the expression of the molybdopterin-containing formate dehydrogenase^{44,45} and Mo- or tungsten (W)-dependent formylmethanofuran dehydrogenase (Fmd and

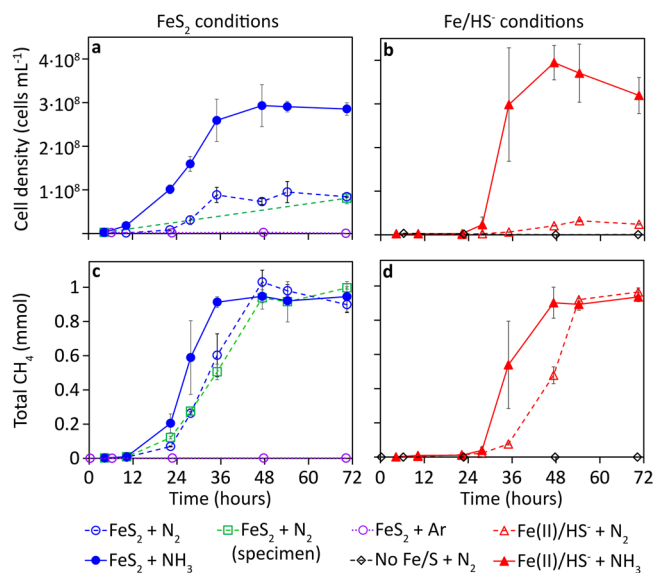


Fig. 1 Growth of *Methanococcus maripaludis* with formate as methanogenesis substrate under nitrogen-fixing and ammonia-amended growth conditions with pyrite or ferrous iron and sulfide as the sole provided iron and sulfur source. Growth and activity were monitored by quantifying cell density (**a**, **b**) and methane production (**c**, **d**) over time, respectively. Panels **a** and **b** and panels **c** and **d** are plotted using the same y-axes, respectively. The data presented are the mean and standard deviation of three biological replicates per condition. ammonia NH_3 , argon Ar, dinitrogen N_2 , ferrous iron Fe(II), methane CH_4 , pyrite FeS_2 , sulfide HS^- .

Fwd, respectively)^{46,47}. Results are discussed as they relate to the potential environmental condition (i.e., euxinic or ferruginous) that would have allowed the O_2 -sensitive Nif enzyme to evolve and function in a methanogen, and ultimately other anaerobes, in the anoxic habitats of early and present-day Earth.

Results and discussion

Nitrogen fixation and Fe/S source affect *Methanococcus maripaludis* S2 (MmS2) Growth and Activity. MmS2 grew in both N_2 -fixing and non- N_2 -fixing (NH_3 -amended) growth conditions when synthetic nanoparticulate FeS_2 or Fe(II)/HS^- were provided as the sole Fe/S sources and with formate as the electron donor and methanogenesis substrate (Fig. 1a–d). Growth did not occur in cultures that were not provided with an Fe/S source, regardless of whether cells were provided with N_2 or NH_3 . Likewise, cultures grown in the absence of NH_3 and under a headspace of argon (Ar) did not grow, regardless of the Fe/S source provided (Fig. 1a, c). Importantly, MmS2 was also able to grow under N_2 -fixing conditions with specimen (63–150 μm grain size) FeS_2 , indicating that a natural (not laboratory-synthesized) form of FeS_2 provides Fe and S during N_2 fixation (Fig. 1a, b). Cell counts and CH_4 measurements were performed infrequently in cultures with specimen FeS_2 since preliminary experiments showed they were sensitive to mechanical disturbance. This may be related to the different geometries of the synthetic nanoparticulate FeS_2 that is composed of small fram-boids with high surface area compared to the large and flat facies of the mostly cubic specimen FeS_2 , which could affect the ability for cells to attach (Supplementary Fig. 1). Nonetheless, these data indicate that both synthetic and natural forms of FeS_2 can serve as the sole Fe/S source in N_2 -fixing MmS2 cells.

The total number of cells produced in the NH_3 -amended cultures was higher relative to N_2 -fixing cultures, regardless of the source of Fe/S provided (Fig. 1a, b). Despite differences in final cell densities, cultures grown under all conditions (except for

negative controls) produced similar amounts of CH_4 by 54 h incubation (Fig. 1c, d). As such, the cell yield (cells per mmol CH_4) in N_2 -fixing cultures was significantly ($p < 0.01$) lower than in NH_3 -amended cultures (Supplementary Fig. 2). This finding is consistent with a nearly three-fold decrease in the cell yield of the methanogen, *Methanothermobacter thermolithotrophicus*, when grown under N_2 -fixing conditions relative to NH_3 -amended conditions⁴⁸. The source of Fe and S provided to MmS2 cultures also had a marked effect on the rate of cell production (Supplementary Table 1) and the total number of cells produced for N_2 -fixing conditions but had minimal effect on NH_3 -amended cultures (Fig. 1a, b). Specifically, N_2 -fixing cultures provided with FeS_2 had a nearly three-fold higher ($p < 0.01$) cell yield than those provided with Fe(II)/HS^- (Supplementary Fig. 2). In contrast to past reports that showed NH_3 -amended cultures of *M. voltae* and *M. barkeri* (both strains MS and Fusaro) achieved similar cell yields when provided with FeS_2 or Fe(II)/HS^- , FeS_2 -grown MmS2 had a yield that was 29% lower than Fe(II)/HS^- -grown cells provided with NH_3 . However, the reduction in cell yield was even more dramatic when N_2 -fixing MmS2 cells were compared, with those provided with Fe(II)/HS^- exhibiting a 92% reduction in yield relative to those provided NH_3 . This demonstrates the energetic burden N_2 fixation places on MmS2 cells and the dependency of this on the Fe/S source provided.

Nitrogen fixation and Fe/S source affect MmS2 cell size. To better understand differences in the growth kinetics and yields observed in cultures of MmS2 grown under N_2 -fixing or NH_3 -amended conditions with FeS_2 or Fe(II)/HS^- as the sole Fe/S source, the size of cells during the log phase in each growth condition was determined using field-emission scanning electron microscopy (FEM). The average size of MmS2 cells was found to be significantly different ($p < 0.05$) for each growth condition, where NH_3 -amended cells grown with Fe(II)/HS^- were the largest followed by N_2 -fixing cells grown with Fe(II)/HS^- . The NH_3 -amended cells grown with FeS_2 were smaller yet and N_2 -fixing cells grown with FeS_2 were the smallest in size among all treatments (Supplementary Table 1).

Cell size is suggested to be positively correlated with cell growth rate (cell divisions hr^{-1}) and/or nutrient availability, although the regulatory mechanisms for cell size are poorly understood across all domains of life^{49,50}. The “growth law” suggests cell size is positively correlated with growth rate⁵⁰; however, this fails to explain the patterns observed here. Diazotrophic MmS2 cells grown on Fe(II)/HS^- had the second largest size but the lowest of the observed growth rates across all four conditions (Supplementary Table 1). Rather, these results indicate that growth on FeS_2 imparts a greater reduction in cell size than N_2 fixation, and that these effects are semi-additive. This is consistent with recent data that suggest that cell size is more of a function of nutrient availability than growth rate alone⁴⁹, with nutrient-limited conditions leading to smaller cell sizes possibly due to the physiological advantage of increased surface area to volume ratios for nutrient transport across the membrane. For example, the diazotrophic marine cyanobacterium, *Crocospaera watsonii*, was demonstrated to undergo a ~2.2-fold reduction in cell volume in response to Fe limitation⁵¹. Similarly, *M. voltae* cells showed a ~3.2-fold reduction in cell volume when grown on FeS_2 relative to Fe(II)/HS^- ³⁹. Proteomic analysis of *M. voltae* cells revealed an up-expression of iron uptake proteins (Feo) when grown with FeS_2 , indicating cells may incorrectly sense Fe(II) limitation due to assimilation of Fe(II) complexed with sulfide ($\text{FeS}_{(\text{aq})}$), despite FeS_2 -grown cells having higher Fe content³⁹. In comparison, N limitation has also been shown to lead to decreased cell size, with ~1.5-to-2.5-fold reduction in cell volume

in heterotrophic bacterioplankton isolates grown under N-limiting conditions^{52,53}. The semi-additive effect of Fe, S, and N sources and availability on MmS2 cell size and growth rate suggest that MmS2 cells are responding to real or perceived limitations of one or more of these elements.

Nitrogen fixation and Fe/S source affect C and N isotope compositions in MmS2 biomass and CH₄. The isotopic composition of C in biomass and CH₄ has been shown to vary with growth rate, substrate availability, and environmental conditions in a variety of methanogen cultures^{54–58}. To further evaluate the effect of N availability and Fe and S source on the phenotype of MmS2, and to confirm N₂ fixation activity, stable isotopes of C ($\delta^{13}\text{C}$) and N ($\delta^{15}\text{N}$) in CH₄ and/or biomass were examined in cultures grown under N₂-fixing or NH₃-amended conditions with either FeS₂ or Fe(II)/HS⁻ provided as the sole Fe/S source.

MmS2 cell biomass had distinctly different $\delta^{15}\text{N}$ values when grown under N₂-fixing vs. NH₃-amended conditions (Fig. 2a). Cells grown under N₂-fixing conditions had similar $\delta^{15}\text{N}$ values of -3.22 ± 0.14 and $-3.16 \pm 0.06\text{‰}$ when provided with Fe(II)/HS⁻ and FeS₂, respectively. These slight differences in $\delta^{15}\text{N}$ values are not statistically significant ($p = 0.55$) and are similar to $\delta^{15}\text{N}$ values of -4‰ previously reported for N₂-fixing *Methanocaldococcus* and *Methanothermococcus* strains isolated from hydrothermal vents⁵⁹. NH₃-amended MmS2 cells grown with Fe(II)/HS⁻ and FeS₂ had nearly identical $\delta^{15}\text{N}$ values of -21.63 ± 0.23

and $-21.61 \pm 0.47\text{‰}$, respectively. Assimilation of NH₃ by microorganisms such as *E. coli* is known to produce biomass with $\delta^{15}\text{N}$ values ranging from -16 to -21‰ under NH₃ replete conditions⁶⁰. The NH₄Cl salt used to cultivate MmS2 had a $\delta^{15}\text{N}$ value of -3.06‰ (Fig. 2a); as such, the fractionation of $\delta^{15}\text{N}$ in biomass would be closer to $\sim -18.6\text{‰}$ and therefore is within the range of expected values for cells assimilating NH₃.

The $\delta^{13}\text{C}$ values for MmS2 biomass were similar for all growth conditions tested (-48 to -50‰), with the exception of biomass grown under N₂-fixing conditions with Fe(II)/HS⁻ (-46‰ ; Fig. 2b). Previous studies have interpreted decreased fractionation of biomass C isotopes in methanogens to indicate lower turnover of C substrates⁵⁴, and this is consistent with the slow growth rate and low cell densities observed in the N₂-fixing condition with Fe(II)/HS⁻. Nonetheless, all biomass $\delta^{13}\text{C}$ values are within the range of values of biomass (range -30 to -49‰) previously determined for a variety of methanogens when grown with various electron donors/carbon sources across a range of cultivation conditions⁵⁴. The $\delta^{13}\text{C}$ values of CH₄ were overall similar (-58 to -64‰) with the exception of N₂-fixing cells provided with Fe(II)/HS⁻, which was heavier (-58‰) but not significantly different ($p = 0.07$) than that of N₂-fixing cells grown with FeS₂ (-60‰) (Fig. 2b). Like the $\delta^{13}\text{C}$ biomass, the $\delta^{13}\text{C}$ of CH₄ is within the range of values (-50 to -100‰) measured for methanogen cultures when grown with a variety of electron donors/methanogenesis substrates across a range of cultivation conditions^{54,55,61}. Together, these results suggest that N₂ fixation impacts the carbon and energy metabolism of MmS2, and this effect is greater when N₂-fixing cells are provided with Fe(II)/HS⁻ when compared to FeS₂. This could be due to competition for molybdate between formate dehydrogenases, nitrogenases, and potentially formylmethanofuran dehydrogenases, which may be amplified by HS⁻-promoted decreases in the availability of Mo (discussed more below). This would be expected to decrease the rate of formate oxidation and CO₂ production, allowing for the passive exchange of intracellular and extracellular CO₂ to have a larger influence on the isotopic composition of CH₄.

In addition to investigating C and N isotopes, the masses of C and N and C/N ratios were determined for biomass samples (Fig. 2a). The C/N ratios were similar across all conditions (range of 3.4 to 3.6), except N₂-fixing MmS2 cells grown on Fe(II)/HS⁻ that had a C/N ratio of 4.3. Previous studies have shown that C/N ratios in cultures of heterotrophic marine bacterioplankton increase by $\sim 40\%$ when limited to fixed N⁵². Furthermore, the C/N ratio of N₂-fixing *Nostoc* cultures increased by 80% under MoO₄²⁻ limitation⁶². The elevated C/N ratio of N₂-fixing MmS2 cells provided with Fe(II)/HS⁻ (Fig. 2a), when considered in light of the low cell yields in this condition (Supplementary Fig. 2), points to N and/or MoO₄²⁻ limitation in these cells. Importantly, differences in the autotrophic pathways used by methanogens (Wood-Ljungdahl) and oxygenic phototrophs (Calvin Cycle) may influence the partitioning of carbon into biomass or CH₄ and may influence the C/N ratios in biomass that are being compared here.

Nitrogen fixation and Fe/S source affect MmS2 gene expression. Shotgun transcriptomics was used to generate gene expression profiles from log-phase cultures of N₂-fixing and NH₃-amended cells provided with FeS₂ or Fe(II)/HS⁻ as the sole Fe/S source (see Supplementary Table 2 for growth data). Differences in gene expression were then used to begin to identify the metabolic/physiological processes that were impacted by the N, Fe, and S sources that were provided. Overall, 1737 unique transcripts were detected among the 1742 protein-coding genes encoded by MmS2 (99.7% of genes had detectable transcripts).

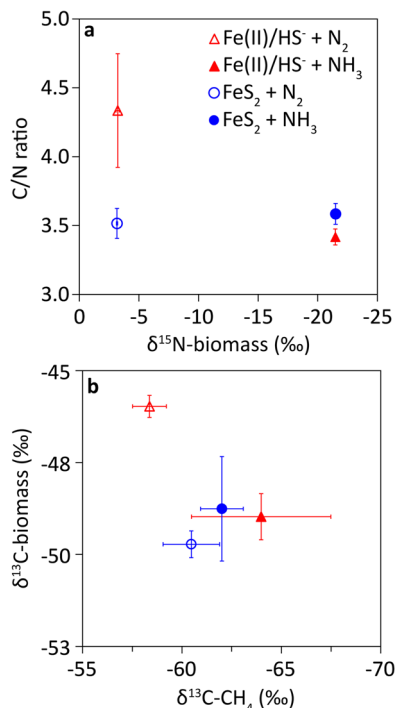


Fig. 2 Isotopic composition of *Methanococcus maripaludis* biomass and methane when grown with formate as methanogenesis substrate under nitrogen-fixing or ammonia-amended conditions with pyrite or ferrous iron and sulfide as the sole provided iron and sulfur source. Mid-log-phase cells (biomass) were analyzed for their carbon-to-nitrogen (C/N) mass ratios and $\delta^{15}\text{N}$ values (a). Biomass and methane were also analyzed for $\delta^{13}\text{C}$ values (b). The legend in a is the same for b. The data presented are the mean and standard deviation of three replicate cultures for all conditions. Isotope results are presented in the delta notation as per mille (‰) values vs. Air ($\delta^{15}\text{N}$) or VPDB ($\delta^{13}\text{C}$). See Supplementary Data 1 for additional data. Ammonia NH₃, dinitrogen N₂, ferrous iron Fe(II), methane CH₄, pyrite FeS₂, sulfide HS⁻.

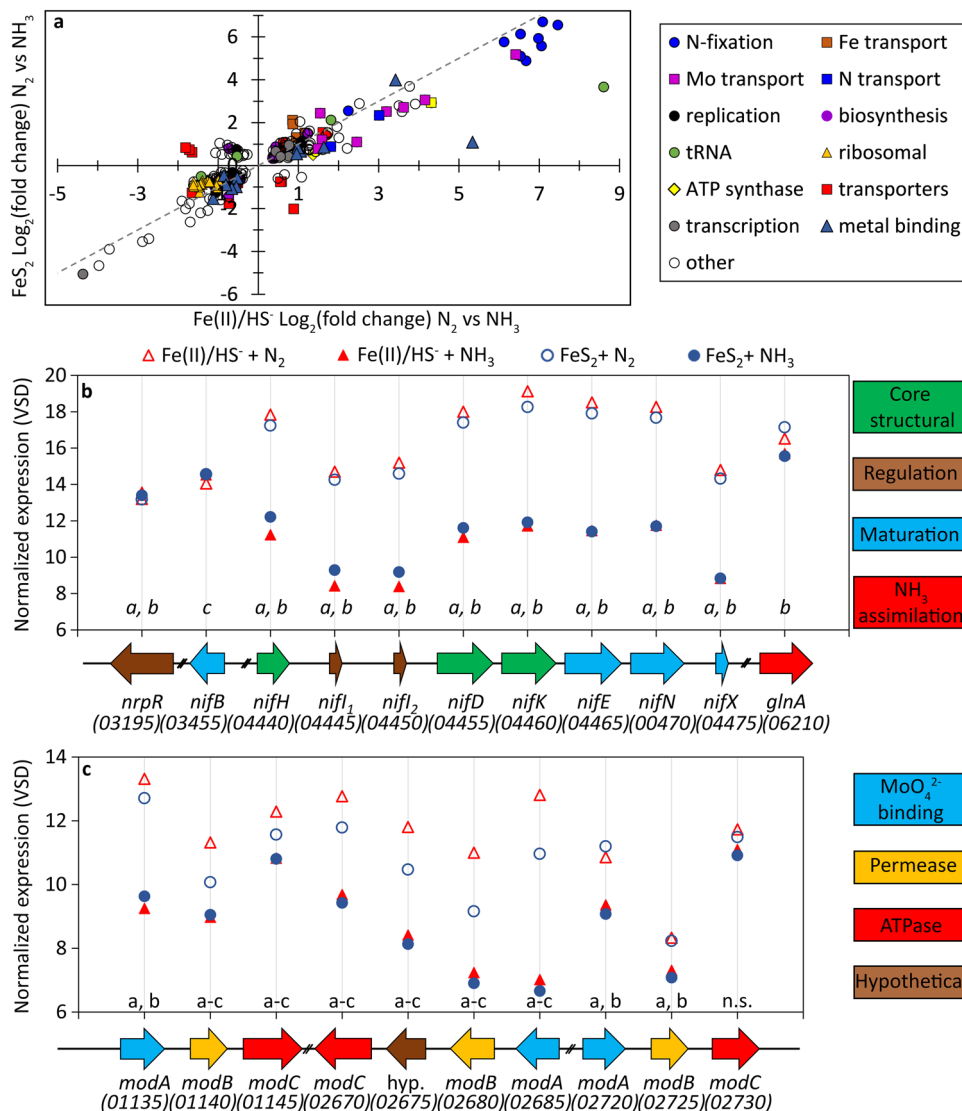


Fig. 3 Differential transcription of genes in *Methanococcus maripaludis* cultures grown under nitrogen-fixing or ammonia-amended conditions with pyrite or ferrous iron and sulfide as the sole provided iron and sulfur source. **a** Transcripts that were significantly differentially expressed ($p < 0.05$, Wald test) for nitrogen-fixing relative to ammonia-amended cells when grown on ferrous iron and sulfide (x-axis) or pyrite (y-axis) shown on a \log_2 -fold-change scale. Positive values indicate higher expression under nitrogen-fixing conditions, and negative values indicate higher expression under ammonia-amended conditions. A gray dashed 1:1 line is provided to ease comparisons based on iron and sulfur source. Mean transcript expression is shown for select genes related to nitrogen fixation (**b**) and molybdenum transport (**c**) that are organized in the order they appear in the genome. Each gene is represented by a color-coded point (**a**) or arrow (**b, c**) with locus tags designated in parentheses (“MMP_RS” has been truncated from the locus designation to conserve space). Genes are colored according to function in the legend to the right of each panel. Each point represents the mean normalized expression of three culture replicates per growth condition. Statistically significant ($p < 0.05$, Wald test) differences in expression for nitrogen-fixing vs. ammonia-amended conditions with ferrous iron and sulfide (**a**) or pyrite (**b**) or between nitrogen-fixing conditions grown with either iron and sulfur source (**c**) are shown above each gene for panels **b** and **c**. ferrous iron Fe(II), pyrite FeS₂, sulfide HS⁻, dinitrogen N₂, ammonia NH₃, no significance, n.s.

Principal component analysis of gene expression profiles revealed that samples clustered according to cultivation conditions (Supplementary Fig. 3). A variety of cellular processes (215 genes) were significantly ($p < 0.05$) differentially regulated between N₂-fixing and NH₃-amended cells grown with either Fe(II)/HS⁻ or FeS₂ (Fig. 3a). The majority of the genes differentially expressed between N₂-fixing and NH₃-amended cells had similar \log_2 -fold-change values for either Fe(II)/HS⁻ or FeS₂ conditions (i.e., these genes fall on a 1:1 line in Fig. 3a), further emphasizing that N₂ fixation induces a significant physiological response regardless of the Fe and S source. Of these genes, those involved in N₂ fixation, molybdenum and iron transport, and metal binding were significantly upregulated under N₂-fixing conditions regardless of Fe

and S source. Conversely, ribosomal genes, genes involved in cellular biosynthesis (e.g., acetyl-CoA synthase), and genome replication (e.g., DNA polymerase) were repressed under N₂-fixing conditions. These results are consistent with decreased growth rates and yields observed for N₂-fixing cells when compared to NH₃-amended cells, regardless of the Fe and S source provided (Fig. 1).

Core *nif* genes are encoded in a single operon in MmS2⁶³ that is transcriptionally regulated by the repressor protein NrpR and 2-oxoglutarate, a signal of N limitation^{64–66}. The *nif* transcriptional regulator, NrpR, was not differentially transcribed based on the N source, which is consistent with previous reports that the activity of this repressor is independent of its levels in the cell

(Fig. 3b)⁶⁷. Genes encoding the core structural components of Nif (*nifHDK*), maturases (*nifENX*), and regulatory proteins (*nifI*, *nifL*) were upregulated in N₂-fixing MmS2 cells relative to NH₃-amended cells and patterns of their expression were generally similar regardless of whether cells were provided with Fe(II)/HS⁻ or FeS₂ (Fig. 3b). A single *nif* gene, *nifB*, falls outside of the *nif* operon and was found to be significantly differentially expressed between N₂-fixing conditions, with Fe(II)/HS⁻-grown cells having slightly lower levels of expression than FeS₂-grown cells. NifB is responsible for the assembly of the FeMo-cofactor precursor, NifB-co, which is then transferred to NifEN where final cofactor maturation takes place through the addition of Mo and homocitrate⁶⁸. It is not clear why the expression of NifB was lower in N₂-fixing conditions in Fe(II)/HS⁻-grown cells. In addition to *nif* genes, expression of glutamine synthase (*glnA*) was elevated in N₂-fixing cells relative to NH₃-amended cells, but this difference was only significant for FeS₂-grown cells. GlnA is an important enzyme for NH₃ assimilation in MmS2⁶⁴, and the higher expression in N₂-fixing FeS₂-grown cells may have contributed to their lower C/N ratios. Collectively, the transcriptomic profiles demonstrate that MmS2 upregulates the expression of genes encoding Nif maturase, Nif structural, and NH₃ assimilation (i.e., GlnA) proteins when fixing N₂ and expression of these genes is generally similar between the Fe/S sources.

Nif is the only nitrogenase encoded by MmS2 and this enzyme is Mo-dependent⁴². In addition, MmS2 encodes a Mo-dependent formate dehydrogenase (Fdh)^{44,45} and both Mo- and W-dependent forms of formylmethanofuran dehydrogenase (Fmd and Fwd, respectively) that are required for methanogenesis with formate^{46,47}. Expression of *fdh* was overall similar among the conditions, with only one subunit encoding gene (*fdhB*; MMP_RS00800) that was significantly upregulated in NH₃-amended conditions relative to N₂-fixing conditions when grown with Fe(II)/HS⁻ (Supplementary Table 3). Interestingly, transcription of *fwd* and *fmd* differed among growth conditions, with three out of seven *fwd* genes (MMP_RS06415–MMP_RS06425) being significantly upregulated under NH₃-amended conditions relative to N₂-fixing conditions in Fe(II)/HS⁻ grown cells; expression of *fwd* genes was similar in NH₃-amended conditions relative to N₂-fixing conditions in FeS₂-grown cells. In the case of *fmd*, the expression of an entire cluster of five *fmd* genes (MMP_RS02690–MMP_RS02710) was significantly upregulated (log₂ fold-change of ~1.5) in N₂-fixing cells relative to NH₃-amended conditions when grown with FeS₂; aside from a single gene *fmdE* (MMP_RS02690), *fmd* transcripts did not differ significantly in N₂-fixing cells relative to NH₃-amended cells when grown with Fe(II)/HS⁻ (Supplementary Table 3). It is unclear why *fwd* was up-expressed under NH₃-amended conditions with Fe(II)/HS⁻ but it could be due to the very high affinity of MoO₄²⁻ for HS⁻ and its low solubility⁶⁹. This, in turn, would increase the bioavailability of tungstate (WO₄²⁻) relative to MoO₄²⁻, that when combined with the higher growth yields in the NH₃-amended conditions with Fe(II)/HS⁻, leads to up-expression of *fwd* transcripts. Similarly, the increased transcription of *fmd* genes under N₂-fixing conditions relative to NH₃-amended conditions on FeS₂ could indicate Mo is more available in FeS₂ growth conditions, with an expression of *fwd* transcripts being unaffected.

Members of both Archaea and Bacteria acquire Mo in the form of MoO₄²⁻ using MoO₄²⁻-specific ABC transporters called Mod⁷⁰. Transcripts for three *mod*-related gene clusters encoded by MmS2 were compared in N₂-fixing and NH₃-amended cells grown with FeS₂ or Fe(II)/HS⁻ (Fig. 3c). Expression of genes comprising all three *mod* gene clusters was upregulated in N₂-fixing cells relative to NH₃-amended cells regardless of Fe/S source. Furthermore, expression of genes comprising two of the three *mod* gene clusters (MMP_RS01135–MMP_RS01145 and

MMP_RS02670–MMP_RS02685) and an annotated NifC-like transporter (MMP_RS08475) were significantly upregulated ($p < 0.05$) in N₂-fixing cells grown with Fe(II)/HS⁻ relative to those grown with FeS₂. These results indicate that N₂ fixation increases the expression of putative MoO₄²⁻ transporters, and this expression is higher in N₂-fixing cells grown with Fe(II)/HS⁻ when compared to those grown with FeS₂. Collectively, these data suggest that MoO₄²⁻ transport is influenced by not only demands associated with Mo-dependent enzymes (Fdh, Fmd, Nif) but also by Fe/S source. More specifically, the results suggest Mo limitation in N₂-fixing cells grown with Fe(II)/HS⁻, possibly due to HS⁻ complexing and/or reacting with Mo^{38,71}.

Abiotic reactions with HS⁻ influence the speciation of Mo. A previous study reported that HS⁻ at a concentration of >6 mM inhibits N₂ fixation in stream sediments⁷². While this effect was attributed to the toxicity of HS⁻ in cells responsible for N₂ fixation, it is plausible that the added HS⁻ influenced the availability of trace metals (e.g., Fe, Mo) required for N₂-fixing cells^{62,73–75}. A similar effect of HS⁻ on metal availability in N₂-fixing MmS2 cultures may explain the lower cell yields and increased expression of Mod genes observed in Fe(II)/HS⁻-grown cells relative to those grown with FeS₂. MoO₄²⁻ is a thiophilic molecule that readily reacts with HS⁻ to form soluble thiomolybdate (MoO_{4-n}S_n²⁻) species that can ultimately be incorporated in sulfide minerals, such as FeS₂^{71,76}. Such thiolation reactions would be expected to occur under the sulfidic (2 mM) cultivation conditions typically used to culture methanogens⁷⁷ and that were utilized herein for the Fe(II)/HS⁻-grown cultures. These euxinic cultivation conditions potentially limited the availability of MoO₄²⁻ such that it did not meet cellular demands.

To begin to examine this hypothesis, the speciation of Mo was tracked in abiotic reactors containing anoxic, base salts medium without added NH₃ or metals. Reactors were amended with various combinations of HS⁻ (2 mM), Fe(II) (25 μM), or FeS₂ (2 mM) to mimic cultivation conditions used in experiments up to this point. To these, Mo was added as MoO₄²⁻ and the concentration of MoO₄²⁻ and its conversion to MoO_{4-n}S_n²⁻ were monitored via colorimetric assays⁷⁸ and UV–Vis spectroscopy⁷¹, respectively. Experiments were performed with 10 μM of MoO₄²⁻ (as opposed to 4 μM used to cultivate MmS2 herein) to increase signal sensitivity such that it was within the dynamic range of the assays that were used.

MoO₄²⁻ concentrations remained at ~8–10 μM in reactors not amended with HS⁻ in the presence or absence of FeS₂ (Supplementary Fig. 4a). As expected, the product of complete thiolation of MoO₄²⁻, tetrathiomolybdate (MoS₄²⁻), was not detected in these conditions throughout the course of the experiment (Supplementary Fig. 4b). In contrast, MoO₄²⁻ concentrations decreased rapidly (within the first 12 h of incubation) when HS⁻ alone or HS⁻ and Fe(II) were added to reactors (Supplementary Fig. 4a). In reactors containing HS⁻, MoS₄²⁻ was rapidly produced (within the first hour of incubation) and MoO₄²⁻ was completely converted to MoS₄²⁻ by 72 h incubation. In reactors containing both HS⁻ and Fe(II), the conversion of MoO₄²⁻ to MoS₄²⁻ was accelerated, and complete conversion occurred within the first 3 h of incubation (Supplementary Fig. 4b). UV–Vis spectroscopy revealed production of MoO_{4-n}S_n²⁻ intermediates in reactors amended with HS⁻ with or without Fe(II) (Supplementary Fig. 5). Ions of MoO₄²⁻/thiomolybdate have a strong affinity for Fe, including Fe in iron sulfides^{79,80}, and it has been shown that these ions readily react to form stable Fe–Mo–S cubane-like structures in sulfur-rich environments⁸⁰. It is possible that the acceleration of MoO₄²⁻ thiolation by Fe(II) in the experiments described here is similarly

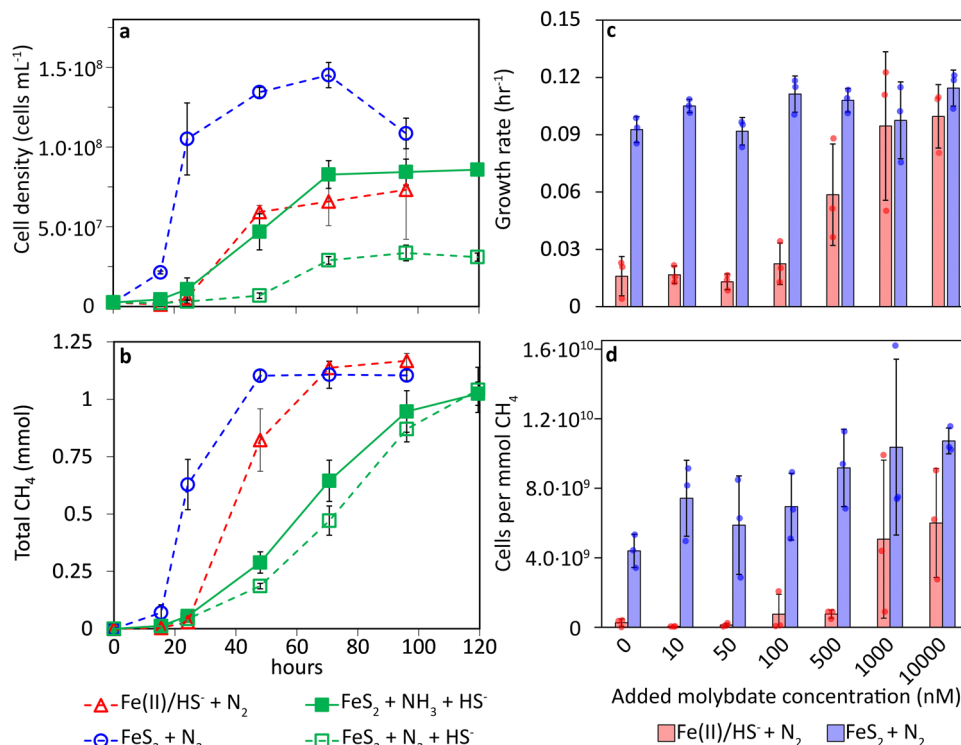


Fig. 4 The effect of added sulfide or molybdenum on the growth of *Methanococcus maripaludis* with formate as methanogenesis substrate under nitrogen-fixing conditions with pyrite or ferrous iron and sulfide as the primary iron and sulfur source. Two mM HS⁻ was added to nitrogen-fixing or ammonia-amended cultures provided with pyrite as the primary iron and sulfur source to test its effect on the production of cells (a) and methane (b). The effect of different molybdate concentrations on the growth rates (c) and yields (d) of cells grown with either pyrite or ferrous iron and sulfide as the sole iron and sulfur source under nitrogen-fixing conditions are shown. Maximal growth rates (calculated from measured cell densities) were determined over a 5-day period for each replicate. The data presented are the mean and standard deviation of three biological replicates per condition. Ammonia NH₃, dinitrogen N₂, ferrous iron Fe(II), methane CH₄, pyrite FeS₂, sulfide HS⁻.

attributable to the formation of stable Fe-Mo-S cubane-like clusters. Regardless, these data indicate that MoO₄²⁻ is readily available in cultures grown with FeS₂, while the predominant forms of Mo in cultures grown with Fe(II)/HS⁻ are a mixture of MoS₄²⁻ and MoO_{4-n}S_n²⁻. This could potentially explain poor growth and up-expression of *mod* genes in N₂-fixing cultures provided with Fe(II)/HS⁻ relative to FeS₂. It is unknown if N₂-fixing MmS2 cells in the Fe(II)/HS⁻ conditions are using sub-micromolar levels of MoO₄²⁻ that are below the detection limit (~1 μM) of the colorimetric assay used herein or if they can use MoO_{4-n}S_n²⁻ (albeit to a limited extent based on growth data) to meet their Mo nutritional demands.

HS⁻ influences the bioavailability of MoO₄²⁻ and MmS2 growth kinetics. To further test the hypothesis that euxinic conditions (i.e., excess HS⁻) limit the availability of MoO₄²⁻ in MmS2 cultures, the growth of N₂-fixing cells provided with Fe(II)/HS⁻ was compared to N₂-fixing cells provided with FeS₂ in the presence or absence of 2 mM added HS⁻. An NH₃-amended MmS2 culture provided with FeS₂ and 2 mM added HS⁻ was also tested. As was observed previously, MmS2 grown with FeS₂ exhibited faster growth and CH₄ production kinetics and generated higher cell yields than cultures provided with Fe(II)/HS⁻ when fixing N₂ (Fig. 4a, b). In comparison, FeS₂-grown cultures with 2 mM added HS⁻, regardless of N source, exhibited significantly slower rates of cell and CH₄ production, demonstrating that HS⁻ decreases the growth of MmS2 in cells provided with FeS₂. While both N₂-fixing and NH₃-amended cultures provided with FeS₂ and 2 mM added HS⁻ conditions grew poorly, N₂-fixing cells were more negatively impacted.

If HS⁻ negatively impacts cellular growth under N₂-fixing conditions through its effect on MoO₄²⁻, it would be expected that cells grown on FeS₂ would have lower requirements for MoO₄²⁻ in solution than Fe(II)/HS⁻-grown cells since relatively small amounts of HS⁻ are released into solution during FeS₂ reduction. Previous experiments performed with H₂-grown, N₂-fixing MmS2 cells provided with Fe(II)/HS⁻ found that >400 nM MoO₄²⁻ was required for growth with an optimum of 4000 nM⁴². These values are much higher than those required of other N₂-fixing organisms. For example, aerobic, N₂-fixing cyanobacteria such as *Anabaena variabilis*⁸¹, as well as anaerobic N₂-fixing purple sulfur bacteria (PSB) inhabiting the interface of oxic/euxinic waters and that serves as a modern analog of the productive continental margins of Proterozoic oceans⁸², can be supported by less than 10 nM MoO₄²⁻. Interestingly, maximum N₂ fixation for the PSB was maximal above the chemocline where HS⁻ was near zero⁸². Thus, it seems incongruous that methanogens would require 40-fold more MoO₄²⁻ than these organisms, despite ancestors of methanogens likely being where Nif originated^{6,9}.

To further test this, formate-grown and N₂-fixing MmS2 cells were provided with a range of MoO₄²⁻ concentrations with Fe(II)/HS⁻ or FeS₂ as the sole Fe/S source. Consistent with previous work⁴², MmS2 grown on Fe(II)/HS⁻ showed little to no growth response in conditions with <100 nM MoO₄²⁻ but growth rates increased substantially when ≥500 nM MoO₄²⁻ was provided (Fig. 4c). Cell yields did not reach maximum levels in Fe(II)/HS⁻-grown cells until >1000 nM MoO₄²⁻ was provided (Fig. 4d). Strikingly, cells provided with FeS₂ grew well under all Mo concentrations tested, including when 0 μM MoO₄²⁻ was added (Fig. 4c). After this experiment, abiotic reactors containing media

and FeS_2 (no MoO_4^{2-} added) were analyzed by ICP-MS and were determined to have background (contaminant) Mo ranging from 10 to 30 nM despite using ACS-grade chemicals and acid-washed glassware. Thus, Fe(II)/HS^- -grown N_2 -fixing cells required >500 nM MoO_4^{2-} to achieve near-optimal growth rates and yields whereas FeS_2 -grown N_2 -fixing cells required <30 nM MoO_4^{2-} .

Collectively, these results suggest that MmS2 cells grown with FeS_2 (in the absence of high concentrations of free HS^-) can access MoO_4^{2-} at nM concentrations that are >10 -fold lower than previously reported for this strain⁴². Further, MmS2 cells can achieve optimal growth rates and yields at MoO_4^{2-} concentrations that are at levels ~ 100 -fold lower than previously reported⁴². Despite similar growth rates for the FeS_2 conditions at different MoO_4^{2-} concentrations, there was a positive trend in the cell yield with increasing MoO_4^{2-} that indicates higher MoO_4^{2-} concentrations are still beneficial to these cells (Fig. 4d). These findings are consistent with other studies that have shown N_2 fixation at low Mo concentrations with cells grown under non-sulfidic conditions^{81,82}. Notably, the low levels (10–30 nM) of MoO_4^{2-} shown to support N_2 fixation herein are similar to the inferred Mo concentrations of Proterozoic oceans^{83–85}. Other studies investigating Mo requirements for other methanogen species fixing N_2 found 1 to 10 μM MoO_4^{2-} to be the optimal concentrations^{86,87}. There is one other example of methanogens fixing N_2 at low (<10 nM) MoO_4^{2-} concentrations; Nishizawa et al. showed that isolates of *Methanocaldococcus* and *Methanothermococcus* from a hydrothermal vent could fix N_2 with as low as 5 nM or 1 μM MoO_4^{2-} , respectively⁵⁹. This indicates that different methanogen species within the same hydrothermal environment (at different temperatures) can have very different Mo requirements. Importantly, these past experiments were all performed in the presence of >1 mM HS^- , necessitating a re-evaluation of methanogens', and other anaerobes', ability to access MoO_4^{2-} in the absence of high HS^- . These data support the hypothesis that N_2 fixation via Nif is more efficient in low HS^- conditions where Mo is more bioavailable.

Ferruginous conditions favor growth of MmS2 under N_2 -fixing conditions. Excess HS^- repressed growth of MmS2 when grown with FeS_2 (euxinic conditions), regardless of the N source provided (Fig. 4). Next, the growth of N_2 -fixing cells was compared in FeS_2 -grown cultures with medium formulations designed to mimic mildly (100 μM added Fe(II)) and highly (1000 μM added Fe(II)) ferruginous conditions and to mimic mildly (100 μM added HS^-) and highly (1000 μM added HS^-) euxinic conditions. Control cultures contained FeS_2 as the sole source of Fe and S. Cell densities and CH_4 concentrations were monitored as growth proxies, and HS^- was measured as a proxy for FeS_2 reduction.

MmS2 cells grew better under the mildly ferruginous condition relative to mildly and highly euxinic conditions, although the highly ferruginous condition caused a longer lag phase (Fig. 5a). Growth of MmS2 cells under euxinic conditions, especially with 1000 μM added HS^- , was greatly diminished relative to cells grown with FeS_2 as the control. Despite the differences in the overall densities of cells at the end of the experiment, all conditions produced similar amounts of CH_4 (Fig. 5b). This led to pronounced differences in final cell yields (Fig. 5d), as well as yields during log phase (Supplementary Fig. 6). In particular, cell yields for the mildly ferruginous condition were the highest even relative to the control condition (FeS_2 only). Again, yields of cells grown in euxinic conditions were significantly lower than those grown in either ferruginous conditions or in the control (FeS_2 only) condition. Together, these data suggest that mildly ferruginous conditions are preferred for N_2 -fixing MmS2 cells.

Total sulfide (HS^- , H_2S , and acid labile iron-sulfide) was measured in non-filtered culture samples as an indicator of FeS_2 reduction⁴¹. Despite all conditions requiring the mobilization of FeS_2 to access either Fe (euxinic conditions), S (ferruginous conditions), or both Fe and S (control condition), the production of total sulfide differed among conditions (Fig. 5c). For FeS_2 alone (control conditions), 34 μmol total sulfide was observed by the end of the experiment, while the mildly euxinic condition produced 46 μmol total sulfide. Accounting for the added HS^- (100 μM , 7.5 μmol), 38 μmol of total sulfide was produced minus what was assimilated by the cells in mildly euxinic conditions. Further, this indicates a similar amount of cellular FeS_2 reduction took place in these two growth conditions; however, more FeS_2 was reduced per cell in the mildly euxinic condition given low cell production. Similarly, in the highly (1000 μM , 75 μmol added HS^-) euxinic condition, 148 μmol total sulfide was measured at the end of the experiment, indicating that more FeS_2 was reduced on a per cell basis than control conditions considering low cell production in the former condition (Fig. 5a). Total sulfide production in cultures grown in ferruginous conditions was far less than control cultures (FeS_2 -only). Specifically, mildly (100 μM added Fe(II)) ferruginous conditions produced only 4 μmol total sulfide, while total sulfide remained undetectable in highly (1000 μM added Fe(II)) ferruginous conditions until the final time point where 0.3 μmol was detected. Thus, the amount of FeS_2 that must be reductively dissolved to meet biosynthetic demands for Fe or S is lower in ferruginous conditions than in euxinic conditions, which may also help to explain better growth under these conditions.

The impact that HS^- had on FeS_2 -grown cells is likely attributable to the complex conditions created when HS^- , FeS_2 , and trace metals (i.e., Mo, Fe(II)) co-occur. High HS^- concentrations decrease the thermodynamic favorability of FeS_2 reduction⁴¹, which might make FeS_2 reduction the rate-limiting process in these cultures and possibly explain the slower production of CH_4 observed in FeS_2 -grown cultures with added HS^- (Figs. 4b and 5b). In addition, high HS^- may reduce the metal availability of not only MoO_4^{2-} , but also Fe(II) that is released during FeS_2 reduction. Spietz et al. describe a model for reductive dissolution of FeS_2 by methanogens wherein FeS_2 reduction releases HS^- into solution and pyrrhotite (Fe_{1-x}S) is precipitated as a secondary phase on the mineral surface⁴¹. Dissolution of Fe_{1-x}S results in the release of Fe(II) (but not HS^-) that can then react with soluble HS^- to form $\text{FeS}_{(\text{aq})}$ clusters, the presumed source of Fe/S for these cells^{39,41}. In abiotic experiments with Fe_{1-x}S sequestered in 100 kDa dialysis membranes, it was shown that dissolution and/or diffusion of Fe from Fe_{1-x}S to the bulk medium was significantly decreased in the presence of 500 μM HS^- when compared to no added HS^- ⁴¹. This may indicate that HS^- increases the rate of $\text{FeS}_{(\text{aq})}$ nucleation and re-precipitation as mackinawite (FeS_{mack}) nanoparticles that are too large to diffuse across the cell membrane. Such particles would be expected to limit Fe (and S) availability to cells⁴¹. These effects of HS^- are presumed to not occur under ferruginous conditions because Fe(II) effectively scrubs HS^- or because cells minimize FeS_2 reduction such that all HS^- released from the process is assimilated. It is also important to consider the tendency for trace metals to become adsorbed onto FeS_2 surfaces that, in turn, reduces their concentration in solution. This is the case for MoS_4^{2-} , the product of complete MoO_4^{2-} thiolation (see above), which more strongly adsorbs to FeS_2 surfaces than MoO_4^{2-} ⁸⁰.

Conversion of FeS_2 to nitrogenase metalloclusters: implications for element cycling in past and contemporary anoxic habitats. Experiments conducted herein were aimed at identifying the most plausible conditions (euxinic or ferruginous) that

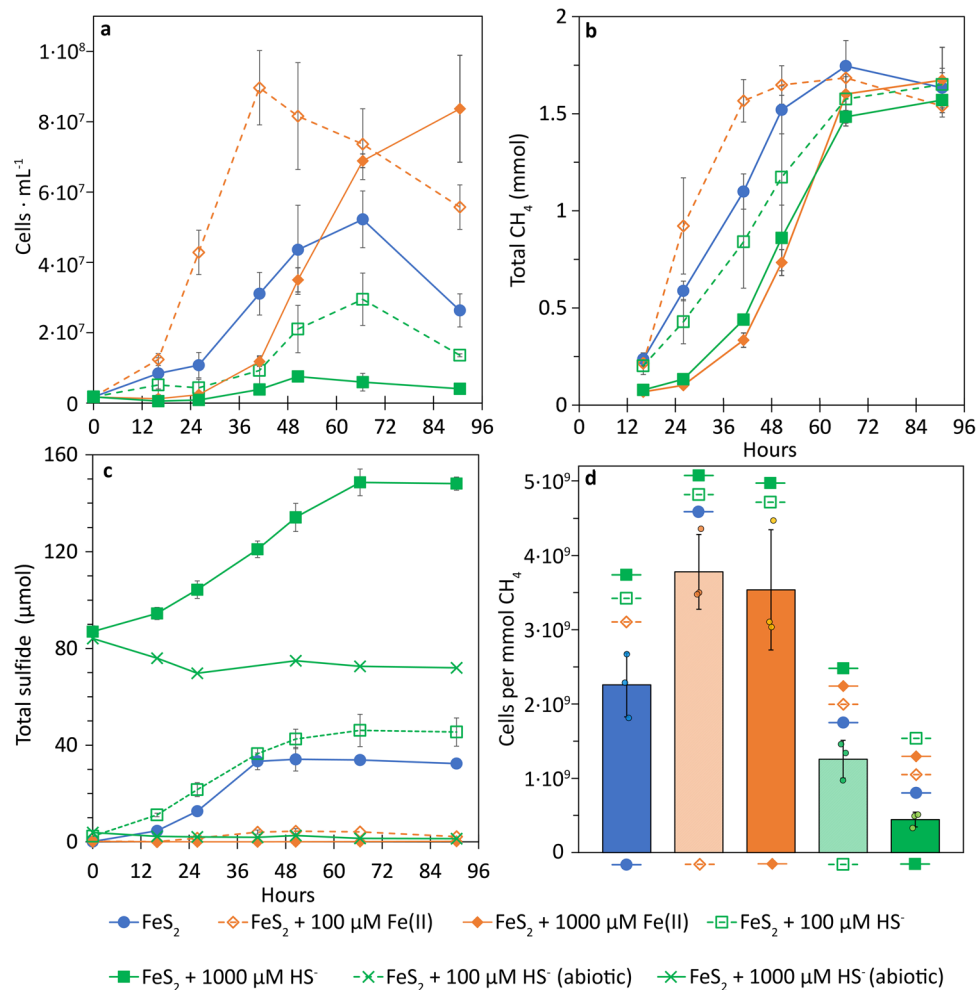


Fig. 5 The effect of excess ferrous iron (Fe(II)) or sulfide (HS⁻) on *Methanococcus maripaludis* S2 (MmS2) under nitrogen-fixing conditions. Production of cells (a), methane, CH₄ (b), and HS⁻ (c) was monitored in cultures of MmS2 provided with 2 mM pyrite (FeS₂) as the sole Fe/S source, with FeS₂ and 100 or 1000 μM of Fe(II), or with FeS₂ and 100 or 1000 μM HS⁻. Cell yields (d) in each growth condition were calculated using the initial and maximum cell and CH₄ concentrations for each replicate. The legend at the bottom of the figure applies to all four panels. Statistically significant ($p < 0.05$, t -test) differences were determined pairwise in panel d and are depicted above each bar using the symbols from the legend to denote the significantly different pairs. The data presented are the mean and standard deviation of three biological replicates per condition. Ferrous iron Fe(II), methane CH₄, pyrite FeS₂, sulfide HS⁻.

would have enabled N₂ fixation via Nif during the early Proterozoic, when phylogenetic data indicate this enzyme evolved^{6–8}, or even in the late Archean, when isotopic data suggest this enzyme or its predecessor evolved^{21,22}. Experiments were conducted with the marine methanogen, MmS2, which harbors a Nif homolog that belongs to the deepest branching Nif lineage^{6,8,9}. Data showed that euxinic conditions (excess of HS⁻ relative to free Fe(II)) negatively affected the growth of N₂-fixing MmS2 cells, regardless of whether they were grown with Fe(II)/HS⁻ or FeS₂. This was shown to be due to the effect of HS⁻ on the speciation and availability of Mo. However, under ferruginous conditions, excess Fe(II) titrates HS⁻ leading to its precipitation as FeS_{mack} and FeS₂ which, in turn, allows Mo to remain bioavailable as MoO₄²⁻. Indeed, the growth rate and yield of N₂-fixing MmS2 cells were significantly higher when cells were grown with FeS₂ and excess Fe(II) (ferruginous conditions) than when grown with i) FeS₂ and excess HS⁻ (euxinic conditions), ii) FeS₂ alone, or iii) under canonical conditions typically used to culture methanogens, excess HS⁻ and Fe(II) (also a euxinic condition).

Collectively, these data indicate that MmS2 prefers FeS₂ over Fe(II)/HS⁻ during growth with formate as methanogenesis

substrate and with N₂ as the sole N source, conditions that increase the demand of Mo via Fdh, Nif, and Fmd. Additionally, cells grew more efficiently with FeS₂ when MoO₄²⁻ was ~100-fold lower in concentration than cells grown with Fe(II)/HS⁻. These data suggest that a ferruginous environment would have favored the function and potentially the origin of Nif on early Earth. In contrast, euxinic conditions pose significant challenges to access thiophilic metals required for N₂-fixing cells in both ancient and modern environments, thus limiting N₂ fixation via Nif. Since metal availability is a major driver of the evolution of metalloenzymes (reviewed in⁸³), we suggest that Nif likely evolved in an environment that favored the availability of Fe and Mo.

Methods

Preparation of minerals. Synthetic FeS₂ was synthesized in an anaerobic chamber by mixing separate solutions of 16.7 g FeSO₄ · 7 H₂O and 17.28 g Na₂S · 9 H₂O each dissolved in 50 mL of anoxic, deionized MilliQ H₂O (MQ) in a 500 mL media bottle. 2.1 g elemental sulfur was then added to the reactor, which was then sealed with a rubber stopper and removed from the anaerobic chamber. The reactor was then incubated for four days at 65 °C followed by another four days at 85 °C. The reactor was then cooled to room temperature and was opened in a chemical fume

hood where the resulting mineral was collected into centrifuge tubes and washed several times aerobically with MQ, 1 M HCl, 6 M HCl, and acetone. Finally, the mineral was washed in sterile, anoxic MQ several times within an anaerobic chamber and transferred into a sterile glass serum bottle as a slurry⁴⁰. Dried specimen FeS₂ was crushed and sieved (63–150 µm particle size) before it was subjected to the same wash series as the synthetic FeS₂. The specimen FeS₂ was then dried under a stream of N₂ and stored in a sterile glass serum bottle until it was weighed in an anaerobic chamber and then added directly to culture bottles. Synthetic FeS₂ was added to prepared culture bottles as a slurry. Minerals were characterized by X-ray diffraction prior to their use in experiments (Supplementary Fig. 7).

Strains and media. *M. maripaludis* strain S2 (MmS2), kindly provided by Dr. Kyle Costa, was grown in Fe- and S-free basal medium that contained (g L⁻¹): NaCl, 21.98; MgCl₂ · 6H₂O, 5.10; NaHCO₃, 5.00; K₂HPO₄, 0.14; KCl, 0.33; CaCl₂ · 2H₂O, 0.10. For NH₃-amended cultures, NH₄Cl was added to a final concentration of 0.50 g L⁻¹. The basal medium was amended with 25 µM FeCl₂ · 4H₂O and 2 mM Na₂S · 9H₂O for Fe(II)/HS⁻-grown cells. Sulfide addition experiments tested the effect of 2 mM HS⁻ during growth on FeS₂. Iron and HS⁻ were added from anoxic, autoclaved stock solutions 30 min. prior to inoculation. For FeS₂ growth conditions, the basal medium was amended with synthetic FeS₂ to a final concentration of 2 mM Fe (0.018 g per 75 mL of media) or with 1.5 g of specimen FeS₂. The higher amount of specimen FeS₂ was added to account for differences in the estimated surface area of in specimen vs. synthetic FeS₂⁴⁰. Basal medium was amended (each 1% v/v final concentration) with a trace element, vitamin, formate, and acetate solutions (Supplementary Table 4). The vitamin solutions were filter-sterilized (0.22 µm) whereas the trace element, formate, and acetate solutions were sterilized individually by autoclaving. All solutions were sparged with filtered (0.22 µm) N₂. N₂ and other gases used in this study were passed over a heated column (300 °C) containing H₂-reduced copper shavings.

To prepare the growth medium, all components, except for NaHCO₃, were dissolved in MQ H₂O and then boiled for less than 1 min. After boiling, the bottle containing the medium was removed from the heat and sealed with a butyl rubber stopper with a metal cannula and vent needle and sparged with N₂ gas for 1 h per liter of medium. After degassing, the bottle was sealed, brought into an anaerobic chamber, and NaHCO₃ was added after cooling. After adding these components, the pH of the medium was adjusted to 7.00 using anoxic 2 M HCl or 1 M NaOH. Seventy-five milliliters of media were dispensed into 165 mL serum bottles that were then sealed with new and freshly boiled 20 mm blue butyl rubber (Bellco, Vineland, NJ) stoppers and aluminum crimp caps. The headspace of the medium bottles was purged with 80:20 N₂:CO₂ for 20 min. The bottles were then autoclaved for 20 min at 123 °C. After autoclaving, FeS₂, Fe(II), HS⁻, trace elements, vitamins, and organics were added to the concentrations indicated above.

Cultivation of MmS2. MmS2 was maintained by twice-weekly transfers in a defined medium with Fe(II)/HS⁻, N₂ gas, and formate. Cultures were inoculated on a 5% v/v basis with cells grown under N₂-fixing conditions and that were provided with Fe(II)/HS⁻. All cells were washed in basal, NH₃-free medium (no additions) by centrifuging at 4696 x g for 20 min at 20 °C in a swing-out bucket rotor for all experiments. The density of an aliquot of the washed cells was then immediately enumerated before they were used as inoculum. Cultures were pressurized to 2.87 atm with either 80:20 N₂:CO₂ or Ar:CO₂. All cultures were incubated statically on their sides at 38 °C in the dark.

Measurement of activity and growth. Headspace gas from microcosms was sampled with an N₂-flushed syringe and stopcock and diluted with ultra-high purity N₂ into CaliBond bags (Calibrated Instruments Inc., Manhasset, NY) prior to CH₄ determination. Liquid samples were taken on the benchtop using an N₂-flushed syringe and needle. CH₄ was quantified by gas chromatography and total sulfide was quantified colorimetrically via the methylene blue assay, as described previously⁴⁰. Cells for direct counting were first fixed for four hrs in 2.5% v/v (final concentration) glutaraldehyde at 4 °C and were then counted using a Petroff-Hausser counting chamber on a Nikon YS100 light microscope with a 100x oil objective lens (Nikon, Tokyo, Japan). Fixed cell samples were concentrated by centrifugation at 15,000 x g for 15 min and resuspended in the basal medium of a sufficient volume to facilitate cell counting.

Molybdate stability and thiolation experiments. To test the stability of MoO₄²⁻ in various medium formulations used herein, 75 mL of NH₃-free base salts medium containing trace elements without MoO₄²⁻, formate, acetate, or vitamins were added to 165 mL serum bottles. Medium preparation was as described above for cultures of MmS2. The headspace composition was 80:20 N₂:CO₂. The medium was amended with Na₂MoO₄ · 4H₂O (10 µM final concentration), Na₂S · 9H₂O (2 mM), FeCl₂ · 4H₂O (25 µM), or synthetic FeS₂ (2 mM). Reactors were incubated at 38 °C in the dark and were transferred to an anaerobic chamber (97.5% N₂, 2.5% H₂) and subsamples for spectroscopy were collected via syringe and needle and placed into disposable plastic cuvettes (1 cm path length) that were sealed with plastic cuvette caps before removing from the anaerobic chamber. The concentration of MoO₄²⁻ was determined colorimetrically using a modified catechol

assay⁷⁸. The assay was modified to increase the concentrations of working solution components four-fold and the sample-to-working solution volume ratio was adjusted to 4:1, with a 1 mL total assay volume that was measured at 400 nm with a Genesys 10 S Vis Spectrophotometer (Thermo Scientific, Waltham, MA). The working solution was prepared and stored in the anaerobic chamber 2-weeks prior to the experiment. For tetrathiomolybdate quantification, 1 mL of the sample was directly measured at 467 nm. UV-Vis scans (300 nm to 525 nm) were performed on a Cary UV-Vis-NIR 6000i spectrophotometer (Agilent Technologies Inc., Santa Clara, CA) using the same samples prepared for tetrathiomolybdate quantification. Sample absorbance values for each assay were compared against a standard curve that was prepared with fresh reagents (Na₂MoO₄ · 4H₂O or MoS₄(NH₄)₂).

Electron microscopy. To characterize the size of cells grown under different conditions, field-emission electron microscopy (FEM) was performed. Five milliliters of cell culture was taken as a subsample from mid-log-phase cultures used in transcriptomics experiments (see below). Cells were fixed for two hrs at room temperature in 2.5% EM-grade glutaraldehyde (Electron Microscopy Sciences, Hatfield, PA) in basal medium. The fixed cells were then filtered onto a previously Au-sputtered 0.2 µm black Isopore polycarbonate filter (MilliporeSigma, Burlington, MA) using gentle vacuum filtration. The cells were then washed by the addition of 10 mL basal medium to the filter. After washing, the cells were subjected to an ethanol dehydration series (by filtration) using molecular grade ethanol (25%, 50%, 70%, 85%, 95%, 100%) and were then stored at 4 °C until FEM was performed at the Imaging and Chemical Analysis Laboratory at Montana State University. Samples were mounted on the FEM holder using double-sided carbon tape and sputtered with a thin film of iridium for conductivity before imaging. FEM was performed using a high-resolution Supra 55VP electron microscope (Zeiss, Thornwood, NY) with a primary electron beam energy of 1 keV at different magnifications. Cell size was determined using ImageJ to manually measure individual cells by recording the length of two normal measurements calibrated to the image scale bar.

Transcriptomics experiments. Shotgun transcriptomics was performed on cells of MmS2 grown under N₂-fixing or NH₃-amended conditions with either Fe(II)/HS⁻ or FeS₂ as the sole Fe/S source. Fifty milliliters of culture were harvested during the mid-log phase in an anaerobic chamber by centrifugation at 4696 x g for 30 min at 4 °C. The supernatant was then discarded, and the tubes were removed from the anaerobic chamber and immediately flash-frozen in liquid N₂. Cell pellets were stored at -80 °C until RNA extraction.

Total RNA was extracted from cell pellets using TRIzol reagent (Invitrogen, Carlsbad, CA) following the manufacturer's protocol with minor modifications. One milliliter of TRIzol was added to cell pellets and the resuspended cells were transferred to Lysis E tubes (MP Biomedicals, Irvine, CA) on ice. The cell samples were mechanically lysed by three cycles of 40 sec of bead beating and 5 min of rest at room temperature (-20 °C). After the lysis procedure, 200 µL of molecular grade chloroform was added, the tubes were mixed by inversion and allowed to incubate for 3 min at room temperature. The tubes were then centrifuged for 15 min at 12,000 x g at 4 °C and the upper aqueous phase containing RNA was transferred by pipette into a clean 2-mL tube. RNA was precipitated by the addition of 0.5 mL of 100% molecular grade isopropanol that had been pre-chilled to 4 °C followed by 10 min incubation on ice. RNA was then pelleted by centrifugation for 10 min at 12,000 x g at 4 °C. The supernatant was removed by pipette, and the RNA was washed in 1 mL of 75 % molecular-grade ethanol. RNA was pelleted by centrifugation for 5 min at 7500 x g at 4 °C, the supernatant was removed, and the RNA pellet was air dried for 10 min. Once dried, the RNA was resuspended in 50 µL of RNA-free H₂O (Fisher Scientific, Waltham, MA) by incubating at 55 °C in a heat block for 10 min. RNA was treated to remove residual DNA by the addition of Turbo DNase (Invitrogen, Waltham, MA) according to the manufacturer's instructions. The RNA was then subjected to a second round of precipitation, washing, drying, and resuspension steps as described above. RNA was quantified using a Qubit 2.0 fluorometer with a Qubit BR RNA kit (Invitrogen) and the quality was assayed using a NanoDrop ND-1000 spectrometer (Thermo Scientific). DNA contamination was checked by performing PCR amplification using archaeal-specific 16S rRNA primers and ensuring no amplification had occurred by gel electrophoresis. The RNA was then sent to the University of Wisconsin's Genome Expression Center for quality control, rRNA depletion using custom *Methanococcus*-specific oligonucleotides (Supplementary Table 5), and sequencing on an Illumina NovaSeq 2x150 bp (Illumina, San Diego, CA).

RNA paired-end reads were processed using default settings in TrimGalore! (https://www.bioinformatics.babraham.ac.uk/projects/trim_galore/), a wrapper that implements CutAdapt⁸⁸ to remove adapter sequences and FastQC (<https://www.bioinformatics.babraham.ac.uk/projects/fastqc/>) to filter reads. Reads were aligned to the reference MmS2 genome (ASM1158v1) using BowTie2⁸⁹. Transcriptonal profiles were generated by read counting for each locus using HTSeq⁹⁰, then normalized and analyzed in DESeq2⁹¹ implemented in R v3.6.0. The RNA-sequencing data reported in this paper have been deposited in the NCBI GEO database (GSE216895).

Isotope analyses. Duplicate cultures of MmS2 were grown (see above) and pooled to provide sufficient sample mass for isotope analyses of cell biomass and CH₄. Cultures were grown with Fe(II)/HS⁻ or FeS₂ under N₂-fixing or NH₃-amended conditions and harvested during the late-log phase of growth. Concentrations of CH₄ were determined from each duplicate and cell densities were determined after the duplicates were combined. Cultures were harvested in an anaerobic chamber after reaching > ~3 × 10⁷ cells per mL by centrifugation in 50 mL centrifuge tubes (Globe Scientific, Mahwah, NJ) for 30 min at 4696 x g at 4 °C. The supernatant was removed using a line and needle under low-vacuum and the cells were resuspended in 8 mL of basal medium and transferred to a 15 mL centrifuge tube (Globe Scientific).

To remove bulk FeS₂ (if present), the sample was underlaid with a Percoll (GE Healthcare, Chicago, IL) working solution with 0.4 M NaCl according to the manufacturer's instructions using a syringe and cannula. The samples were then spun at 2000 x g in a swing-out bucket rotor for 20 min at 4 °C. The overlying aqueous phase containing cells was removed by pipette and transferred to a clean 50 mL centrifuge tube, to which ~40 mL of fresh basal medium was added and the tubes were mixed by vortex. The tubes were then spun for 30 min at 4696 x g at 4 °C to pellet the cells away from any residual Percoll. The supernatant was then removed by vacuum, and the cell pellets were resuspended in 1.5 mL of basal medium and transferred into 2.0 mL screw-top microcentrifuge tubes (Thermo Scientific). A subsample (10 µL) of cells was taken and diluted for cell enumeration after processing. Biomass was concentrated by centrifugation for 20 min at 15,000 x g at 4 °C in a fixed-angle rotor, and the supernatant was removed by pipette.

Cell pellets were frozen at -80 °C until shipment to Utah State University Geosciences for C and N stable isotope analyses. Cell pellets were dried aerobically by incubating for 16 h at 60 °C in a drying oven. Once dried, biomass was scraped out of the tubes, weighed, and further prepared for analysis by grinding to a powder and transferring into tin capsules. Isotope analysis of δ¹⁵N (vs. AIR) and δ¹³C (vs. VPDB) values was then performed by combustion and gas chromatography of the biomass samples at 1000 °C using a Costech 4010 Elemental Analyzer coupled with a Thermo Scientific Delta V Advantage isotope ratio mass spectrometry (GC-IRMS). For δ¹³C analysis of CH₄, gas samples from cultures used in the above isotope experiments were shipped to Northern Arizona University and analyzed on a Picarro G2201-I cavity ring-down spectrometer. A commercial δ¹³C -60‰ (vs. VPDB) CH₄ standard (Airgas, Plumsteadville, PA) served as a calibration standard in addition to methane-free air "zero air" for Picarro analyses.

Statistics and reproducibility. All data shown are mean values of at least three independent replicates, with error bars showing the standard deviation of the replicates. Independent Student's *t*-tests were used to calculate *p*-values reported herein for all experiments except for transcriptomics experiments, for which *p*-values were determined by a Wald test calculated in the *DEseq2* package implemented in R. Results were considered significantly different when *p* < 0.05.

Reporting summary. Further information on research design is available in the Nature Portfolio Reporting Summary linked to this article.

Data availability

All data generated or analyzed during this study are included in this published article and its Supplementary Materials. Numerical and replicate data used for all figures are provided in Supplementary Data 1. Sequencing data from transcriptomics experiments are available through the NCBI Gene Expression Omnibus under the accession ID GSE216895. All other data are available from the corresponding author upon reasonable request.

Received: 10 December 2022; Accepted: 21 July 2023;

Published online: 31 July 2023

References

- LeBauer, D. S. & Treseder, K. K. Nitrogen limitation of net primary productivity in terrestrial ecosystems is globally distributed. *Ecology* **89**, 371–379 (2008).
- Yung, Y. L. & McElroy, M. B. Fixation of nitrogen in the prebiotic atmosphere. *Science* **203**, 1002–1004 (1979).
- Kasting, J. F. & Walker, J. C. G. Limits on oxygen concentrations in the prebiological atmosphere and the rate of abiotic nitrogen fixation. *J. Geophys. Res.* **86**, 1147–1158 (1981).
- Howarth, R. W. Nutrient limitation of net primary production in marine ecosystems. *Annu. Rev. Ecol. Syst.* **19**, 89–110 (1988).
- Joerger, R. D. & Bishop, P. E. Bacterial alternative nitrogen fixation systems. *Crit. Rev. Microbiol.* **16**, 1–14 (1988).
- Boyd, E. S. et al. A late methanogen origin for molybdenum-dependent nitrogenase. *Geobiology* **9**, 221–232 (2011).
- Raymond, J., Siefert, J. L., Staples, C. R. & Blankenship, R. E. The natural history of nitrogen fixation. *Mol. Biol. Evol.* **21**, 541–554 (2004).
- Boyd, E. & Peters, J. New insights into the evolutionary history of biological nitrogen fixation. *Front. Microbiol.* **4**, 201 (2013).
- Boyd, E. S., Hamilton, T. L. & Peters, J. W. An alternative path for the evolution of biological nitrogen fixation. *Front. Microbiol.* **2**, 205 (2011).
- Rubio, L. M. & Ludden, P. W. Biosynthesis of the iron-molybdenum cofactor of nitrogenase. *Annu. Rev. Microbiol.* **62**, 93–111 (2008).
- Lancaster, K. M. et al. X-ray emission spectroscopy evidences a central carbon in the nitrogenase iron-molybdenum cofactor. *Science* **334**, 974–977 (2011).
- Chan, M. K., Kim, J. & Rees, D. C. The nitrogenase FeMo-cofactor and P-cluster pair: 2.2 Å resolution structures. *Science* **260**, 792–794 (1993).
- Seefeldt, L. C., Hoffman, B. M. & Dean, D. R. Mechanism of Mo-dependent nitrogenase. *Annu. Rev. Biochem.* **78**, 701–722 (2009).
- Einsle, O. & Rees, D. C. Structural enzymology of nitrogenase enzymes. *Chem. Rev.* **120**, 4969–5004 (2020).
- Danyal, K., Dean, D. R., Hoffman, B. M. & Seefeldt, L. C. Electron transfer within nitrogenase: evidence for a deficit-spending mechanism. *Biochemistry* **50**, 9255–9263 (2011).
- Boyd, E. S. et al. Evolution of molybdenum nitrogenase during the transition from anaerobic to aerobic metabolism. *J. Bacteriol.* **197**, 1690–1699 (2015).
- Shock, E. L. & Boyd, E. S. Principles of geobiochemistry. *Elements* **11**, 395–401 (2015).
- Zheng, K., Ngo, P. D., Owens, V. L., Yang, X. & Mansoorabadi, S. O. The biosynthetic pathway of coenzyme F₄₃₀ in methanogenic and methanotrophic archaea. *Science* **354**, 339–342 (2016).
- Moore, S. J. et al. Elucidation of the biosynthesis of the methane catalyst coenzyme F₄₃₀. *Nature* **543**, 78–82 (2017).
- Allen, K. D., Wegener, G. & White, R. H. Discovery of multiple modified F₄₃₀ coenzymes in methanogens and anaerobic methanotrophic archaea suggests possible new roles for F₄₃₀ in nature. *Appl. Environ. Microbiol.* **80**, 6403–6412 (2014).
- Stüeken, E. E., Buick, R., Guy, B. M. & Koehler, M. C. Isotopic evidence for biological nitrogen fixation by molybdenum-nitrogenase from 3.2 Gyr. *Nature* **520**, 666–669 (2015).
- Garvin, J., Buick, R., Anbar, A. D., Arnold, G. L. & Kaufman, A. J. Isotopic evidence for an aerobic nitrogen cycle in the latest Archean. *Science* **323**, 1045–1048 (2009).
- Dean, D. R., Bolin, J. T. & Zheng, L. Nitrogenase metalloclusters: structures, organization, and synthesis. *J. Bacteriol.* **175**, 6737–6744 (1993).
- Canfield, D. E., Glazer, A. N. & Falkowski, P. G. The evolution and future of Earth's nitrogen cycle. *Science* **330**, 192–196 (2010).
- Mus, F., Colman, D. R., Peters, J. W. & Boyd, E. S. Geobiological feedbacks, oxygen, and the evolution of nitrogenase. *Free Radical Biol. Med.* **140**, 250–259 (2019).
- Canfield, D. E. et al. Ferruginous conditions dominated later Neoproterozoic deep-water chemistry. *Science* **321**, 949–952 (2008).
- Poulton, S. W. & Canfield, D. E. Ferruginous conditions: a dominant feature of the ocean through Earth's history. *Elements* **7**, 107–112 (2011).
- Walker, J. C. & Brimblecombe, P. Iron and sulfur in the pre-biologic ocean. *Precambrian Res.* **28**, 205–222 (1985).
- Holland, H. D. The oceans: a possible source of iron in iron-formations. *Econ. Geol.* **68**, 1169–1172 (1973).
- Planavsky, N. J. et al. Widespread iron-rich conditions in the mid-Proterozoic ocean. *Nature* **477**, 448–451 (2011).
- Reinhard, C. T., Raiswell, R., Scott, C., Anbar, A. D. & Lyons, T. W. A late Archean sulfidic sea stimulated by early oxidative weathering of the continents. *Science* **326**, 713–716 (2009).
- Fakhraee, M., Hancisse, O., Canfield, D. E., Crowe, S. A. & Kasev, S. Proterozoic seawater sulfate scarcity and the evolution of ocean-atmosphere chemistry. *Nat. Geosci.* **12**, 375–380 (2019).
- Arnold, G. L., Anbar, A. D., Barling, J. & Lyons, T. W. Molybdenum isotope evidence for widespread anoxia in mid-Proterozoic oceans. *Science* **304**, 87–90 (2004).
- Anbar, A. D. & Knoll, A. H. Proterozoic ocean chemistry and evolution: a bioinorganic bridge? *Science* **297**, 1137–1142 (2002).
- Rickard, D. & Luther, G. W. Chemistry of iron sulfides. *Chem. Rev.* **107**, 514–562 (2007).
- Berner, R. A. Sedimentary pyrite formation: an update. *Geochim. Cosmochim. Acta* **48**, 605–615 (1984).
- Schoonen, M. A. A. & Barnes, H. L. Reactions forming pyrite and marcasite from solution: II. Via FeS precursors below 100 °C. *Geochim. Cosmochim. Acta* **55**, 1505–1514 (1991).

38. Helz, G. R. et al. Mechanism of molybdenum removal from the sea and its concentration in black shales: EXAFS evidence. *Geochim. Cosmochim. Acta* **60**, 3631–3642 (1996).
39. Payne, D. et al. Examining pathways of iron and sulfur acquisition, trafficking, deployment, and storage in mineral-grown methanogen cells. *J. Bacteriol.* **203**, 1–18 (2021).
40. Payne, D., Spietz, R. L. & Boyd, E. S. Reductive dissolution of pyrite by methanogenic archaea. *ISME J.* **15**, 3498–3507 (2021).
41. Spietz, R. L. et al. Investigating abiotic and biotic mechanisms of pyrite reduction. *Front. Microbiol.* **13**, 878387 (2022).
42. Kessler, P. S., McLarnan, J. & Leigh, J. A. Nitrogenase phylogeny and the molybdenum dependence of nitrogen fixation in *Methanococcus maripaludis*. *J. Bacteriol.* **179**, 541–543 (1997).
43. Hamilton, T. L. et al. Transcriptional profiling of nitrogen fixation in *Azotobacter vinelandii*. *J. Bacteriol.* **193**, 4477–4486 (2011).
44. May, H. D., Schauer, N. L. & Ferry, J. G. Molybdopterin cofactor from *Methanobacterium formicicum* formate dehydrogenase. *J. Bacteriol.* **166**, 500–504 (1986).
45. Wood, G. E., Haydock, A. K. & Leigh, J. A. Function and regulation of the formate dehydrogenase genes of the methanogenic archaeon *Methanococcus maripaludis*. *J. Bacteriol.* **185**, 2548–2554 (2003).
46. Bertram, P. A., Schmitz, R. A., Linder, D. & Thauer, R. K. Tungstate can substitute for molybdate in sustaining growth of *Methanobacterium thermoautotrophicum*. Identification and characterization of a tungsten isoenzyme of formylmethanofuran dehydrogenase. *Arch. Microbiol.* **161**, 220–228 (1994).
47. Schmitz, R. A., Albracht, S. P. & Thauer, R. K. A molybdenum and a tungsten isoenzyme of formylmethanofuran dehydrogenase in the thermophilic archaeon *Methanobacterium wolfei*. *Eur. J. Biochem.* **209**, 1013–1018 (1992).
48. Belay, N., Sparling, R. & Daniels, L. Dinitrogen fixation by a thermophilic methanogenic bacterium. *Nature* **312**, 286–288 (1984).
49. Vadia, S. & Levin, P. A. Growth rate and cell size: a re-examination of the growth law. *Curr. Opin. Microbiol.* **24**, 96–103 (2015).
50. Schaechter, M., MaalØe, O. & Kjeldgaard, N. O. Dependency on medium and temperature of cell size and chemical composition during balanced growth of *Salmonella typhimurium*. *Microbiology* **19**, 592–606 (1958).
51. Jacq, V., Ridame, C., L'Helguen, S., Kaczmar, F. & Salot, A. Response of the unicellular diazotrophic cyanobacterium *Crocosphaera watsonii* to iron limitation. *PLoS ONE* **9**, e86749–e86749 (2014).
52. Vrede, K., Heldal, M., Norland, S. & Bratbak, G. Elemental composition (C, N, P) and cell volume of exponentially growing and nutrient-limited bacterioplankton. *Appl. Environ. Microbiol.* **68**, 2965–2971 (2002).
53. Mårdén, P., Tunlid, A., Malmcrona-Friberg, K., Odham, G. & Kjelleberg, S. Physiological and morphological changes during short term starvation of marine bacterial isolates. *Arch. Microbiol.* **142**, 326–332 (1985).
54. House, C. H., Schopf, J. W. & Stetter, K. O. Carbon isotopic fractionation by Archaeans and other thermophilic prokaryotes. *Org. Geochem.* **34**, 345–356 (2003).
55. Botz, R., Pokojski, H.-D., Schmitt, M. & Thomm, M. Carbon isotope fractionation during bacterial methanogenesis by CO₂ reduction. *Org. Geochem.* **25**, 255–262 (1996).
56. Fuchs, G., Thauer, R., Ziegler, H. & Stichler, W. Carbon isotope fractionation by *Methanobacterium thermoautotrophicum*. *Arch. Microbiol.* **120**, 135–139 (1979).
57. Kleikemper, J., Schroth, M. H., Bernasconi, S. M., Brunner, B. & Zeyer, J. Sulfur isotope fractionation during growth of sulfate-reducing bacteria on various carbon sources. *Geochim. Cosmochim. Acta* **68**, 4891–4904 (2004).
58. Topçuoğlu, B. D., Meydan, C., Nguyen, T. B., Lang, S. Q. & Holden, J. F. Growth kinetics, carbon isotope fractionation, and gene expression in the hyperthermophile *Methanocaldococcus jannaschii* during hydrogen-limited growth and interspecies hydrogen transfer. *Appl. Environ. Microbiol.* **85**, e00180–00119 (2019).
59. Nishizawa, M., Miyazaki, J., Makabe, A., Koba, K. & Takai, K. Physiological and isotopic characteristics of nitrogen fixation by hyperthermophilic methanogens: Key insights into nitrogen anabolism of the microbial communities in Archean hydrothermal systems. *Geochim. Cosmochim. Acta* **138**, 117–135 (2014).
60. Vo, J., Inwood, W., Hayes, J. M. & Kustu, S. Mechanism for nitrogen isotope fractionation during ammonium assimilation by *Escherichia coli* K12. *Proc. Natl Acad. Sci. USA* **110**, 8696 (2013).
61. Miller, H. M. et al. Large carbon isotope variability during methanogenesis under alkaline conditions. *Geochim. Cosmochim. Acta* **237**, 18–31 (2018).
62. Glass, J. B., Wolfe-Simon, F., Elser, J. J. & Anbar, A. D. Molybdenum-nitrogen co-limitation in freshwater and coastal heterocystous cyanobacteria. *Limnol. Oceanogr.* **55**, 667–676 (2010).
63. Kessler, P. S., Blank, C. & Leigh, J. A. The *nif* gene operon of the methanogenic archaeon *Methanococcus maripaludis*. *J. Bacteriol.* **180**, 1504–1511 (1998).
64. Lie, T. J. & Leigh, J. A. Regulatory response of *Methanococcus maripaludis* to alanine, an intermediate nitrogen source. *J. Bacteriol.* **184**, 5301–5306 (2002).
65. Cohen-Kupiec, R., Marx, C. J. & Leigh, J. A. Function and regulation of *glnA* in the methanogenic archaeon *Methanococcus maripaludis*. *J. Bacteriol.* **181**, 256–261 (1999).
66. Lie, T. J., Wood, G. E. & Leigh, J. A. Regulation of *nif* expression in *Methanococcus maripaludis*: roles of the euryarchaeal repressor NrpR, 2-oxoglutarate, and two operators. *J. Biol. Chem.* **280**, 5236–5241 (2005).
67. Lie, T. J. & Leigh, J. A. A novel repressor of *nif* and *glnA* expression in the methanogenic archaeon *Methanococcus maripaludis*. *Mol. Microbiol.* **47**, 235–246 (2003).
68. Hu, Y. & Ribbe, M. W. Biosynthesis of the metalloclusters of nitrogenases. *Annu. Rev. Biochem.* **85**, 455–483 (2016).
69. Stiefel, E. L. in *Metal Ions in Biological Systems*. Vol. 39 (eds Sigel, A. & Sigel, H.) 29 (CRC Press, Boca Raton, FL, 2002).
70. Zhang, Y., Rump, S. & Gladyshev, V. N. Comparative genomics and evolution of molybdenum utilization. *Coord. Chem. Rev.* **255**, 1206–1217 (2011).
71. Erickson, B. E. & Helz, G. R. Molybdenum(VI) speciation in sulfidic waters: Stability and lability of thiomolybdates. *Geochim. Cosmochim. Acta* **64**, 1149–1158 (2000).
72. Tam, T., Mayfield, C. I., Inniss, W. E. & Knowles, R. Effect of sulfide on nitrogen fixation in a stream sediment-water system. *Appl. Environ. Microbiol.* **43**, 1076–1079 (1982).
73. Tuit, C., Waterbury, J. & Ravizza, G. Diel variation of molybdenum and iron in marine diazotrophic cyanobacteria. *Limnol. Oceanogr.* **49**, 978–990 (2004).
74. Saito, M. A. et al. Iron conservation by reduction of metalloenzyme inventories in the marine diazotroph *Crocosphaera watsonii*. *Proc. Natl Acad. Sci. USA* **108**, 2184 (2011).
75. Naito, T., Sachurongui, Ueki, M. & Maeda, I. Light-enhanced bioaccumulation of molybdenum by nitrogen-deprived recombinant anoxygenic photosynthetic bacterium *Rhodospseudomonas palustris*. *Biosci. Biotechnol. Biochem.* **80**, 407–413 (2016).
76. Phillips, R. & Xu, J. A critical review of molybdenum sequestration mechanisms under euxinic conditions: Implications for the precision of molybdenum paleoredox proxies. *Earth Sci. Rev.* **221**, 103799 (2021).
77. Liu, Y., Beer, L. L. & Whitman, W. B. Methanogens: a window into ancient sulfur metabolism. *Trends Microbiol.* **20**, 251–258 (2012).
78. Seifert, S. & Novic, B. Colorimetric determination of molybdate with catechol. *Anal. Chem.* **23**, 188–189 (1951).
79. Xu, N., Christodoulatos, C. & Braida, W. Adsorption of molybdate and tetrathiomolybdate onto pyrite and goethite: effect of pH and competitive anions. *Chemosphere* **62**, 1726–1735 (2006).
80. Bostick, B. C., Fendorf, S. & Helz, G. R. Differential adsorption of molybdate and tetrathiomolybdate on pyrite (FeS₂). *Environ. Sci. Technol.* **37**, 285–291 (2003).
81. Zerkle, A. L., House, C. H., Cox, R. P. & Canfield, D. E. Metal limitation of cyanobacterial N₂ fixation and implications for the Precambrian nitrogen cycle. *Geobiology* **4**, 285–297 (2006).
82. Philippi, M. et al. Purple sulfur bacteria fix N₂ via molybdenum-nitrogenase in a low molybdenum Proterozoic ocean analogue. *Nat. Commun.* **12**, 4774 (2021).
83. Anbar, A. D. Elements and evolution. *Science* **322**, 1481–1483 (2008).
84. Scott, C. et al. Tracing the stepwise oxygenation of the Proterozoic ocean. *Nature* **452**, 456–459 (2008).
85. Collier, R. W. Molybdenum in the Northeast Pacific Ocean. *Limnol. Oceanogr.* **30**, 1351–1354 (1985).
86. Scherer, P. Vanadium and molybdenum requirement for the fixation of molecular nitrogen by two *Methanosarcina* strains. *Arch. Microbiol.* **151**, 44–48 (1988).
87. Maslač, N., Sidhu, C., Teeling, H. & Wagner, T. Comparative transcriptomics sheds light on remodeling of gene expression during diazotrophy in the thermophilic methanogen *Methanothermococcus thermolithotrophicus*. *mBio* **13**, e02443–02422 (2022).
88. Martin, M. Cutadapt removes adapter sequences from high-throughput sequencing reads. *EMBNET J.* **17**, 3 (2011).
89. Langmead, B. & Salzberg, S. L. Fast gapped-read alignment with Bowtie 2. *Nat. Methods* **9**, 357–359 (2012).
90. Anders, S., Pyl, P. T. & Huber, W. HTSeq—a Python framework to work with high-throughput sequencing data. *Bioinformatics* **31**, 166–169 (2015).
91. Love, M. I., Huber, W. & Anders, S. Moderated estimation of fold change and dispersion for RNA-seq data with DESeq2. *Genome Biol.* **15**, 550 (2014).

Acknowledgements

This work was supported by the Division of Chemical Sciences, Geosciences, and Biosciences, Office of Basic Energy Sciences of the U.S. Department of Energy through Grant DE-SC0020246 to R.L.S. and E.S.B.

Author contributions

D.P.: contributed to the experimental design, conducting experiments, and writing of the manuscript. R.L.S.: contributed to the experimental design, conducting experiments, and writing of the manuscript. D.L.N.: contributed to the experimental design, conducting experiments, and writing of the manuscript. P.D.: contributed to the experimental design, conducting experiments, and writing of the manuscript. E.S.B.: contributed to the experimental design and writing of the manuscript.

Competing interests

The authors declare no competing interests.

Additional information

Supplementary information The online version contains supplementary material available at <https://doi.org/10.1038/s42003-023-05163-9>.

Correspondence and requests for materials should be addressed to Eric S. Boyd.

Peer review information *Communications Biology* thanks Masaru Nobu, Tom Jilbert, and the other anonymous reviewer for their contribution to the peer review of this work. Primary handling editors: Anna Heintz-Buschart and David Favero.

Reprints and permission information is available at <http://www.nature.com/reprints>

Publisher's note Springer Nature remains neutral with regard to jurisdictional claims in published maps and institutional affiliations.



Open Access This article is licensed under a Creative Commons Attribution 4.0 International License, which permits use, sharing, adaptation, distribution and reproduction in any medium or format, as long as you give appropriate credit to the original author(s) and the source, provide a link to the Creative Commons licence, and indicate if changes were made. The images or other third party material in this article are included in the article's Creative Commons licence, unless indicated otherwise in a credit line to the material. If material is not included in the article's Creative Commons licence and your intended use is not permitted by statutory regulation or exceeds the permitted use, you will need to obtain permission directly from the copyright holder. To view a copy of this licence, visit <http://creativecommons.org/licenses/by/4.0/>.

© The Author(s) 2023